*Supplement of*

# Contribution of brown carbon on light absorption in emissions of European residential biomass combustion appliances

Satish Basnet[1], Anni Hartikainen[1], Aki Virkkula[2], Pasi Yli-Pirilä[1], Miika Kortelainen[1], Heikki Suhonen[1], Laura Kilpeläinen[1], Mika Ihalainen[1], Sampsa Väätäinen[1], Juho Louhisalmi[1], Markus Somero[1], Jarkko Tissari[1], Gert Jakobi[3,4], Ralf Zimmermann[3,4], Antti Kilpeläinen[5] and Olli Sippula[1,6]

[1]Department of Environmental and Biological Sciences, University of Eastern Finland, FI-70211, Kuopio, Finland
[2]Atmospheric Composition Research, Finnish Meteorological Institute, Helsinki, Finland
[3] Department of Analytical and Technical Chemistry, University of Rostock, DE-18059, Rostock, Germany
[4]Joint Mass Spectrometry Centre, Comprehensive Molecular Analytics, Helmholtz Zentrum München, DE-85764, Neuherberg, German
[5]School of Forest Sciences, University of Eastern Finland, FI-80101, Joensuu, Finland
[6]Department of Chemistry, University of Eastern Finland, FI-80101, Joensuu, Finland

*Correspondence to*: Satish Basnet (satish.basnet@uef.fi), Anni Hartikainen (anni.hartikainen@uef.fi), Olli Sippula (olli.sippula@uef.fi)

**Table S1.** Dry fuel properties of fuel types used in experiments.

| Parameter | birch log | birch log | birch log | birch log | beech log | spruce log | pine log | softwood pellets | peat |
|---|---|---|---|---|---|---|---|---|---|
| moisture (%) | 7.20 | 11.00 | 18.00 | 28.00 | 9.00 | 7.40 | 6.10 | 7.30 | 17.90 |
| ash content @ 550 °C (% (w/w, dry)) | 0.69 | 0.69 | 0.69 | 0.69 | 1.30 | 0.58 | 0.45 | 0.36 | 4.90 |
| carbon (% (w/w, dry)) | 51.00 | 51.00 | 51.00 | 51.00 | 50.30 | 52.00 | 51.10 | 51.70 | 56.20 |
| hydrogen (% (w/w, dry)) | 6.00 | 6.00 | 6.00 | 6.00 | 5.80 | 5.90 | 6.40 | 6.00 | 5.70 |
| nitrogen (% (w/w, dry)) | 0.40 | 0.40 | 0.40 | 0.40 | 0.36 | 0.36 | < 0.05 | 0.29 | 2.01 |
| oxygen (% (w/w, dry)) | 41.90 | 41.90 | 41.90 | 41.90 | 42.30 | 41.10 | 42.0 | 41.60 | - |
| sulphur (% (w/w, dry)) | 0.006 | 0.006 | 0.006 | 0.006 | 0.037 | 0.009 | <0.005 | 0.006 | 0.22 |
| chlorine (% (w/w, dry)) | <0.005 | <0.005 | <0.005 | <0.005 | <0.005 | 0.005 | <0.005 | 0.006 | 0.023 |
| Net calorific value (MJ per kg fuel) | 18.14 | 18.14 | 18.14 | 18.14 | 17.79 | 18.64 | 19.32 | 18.38 | 22.92 |
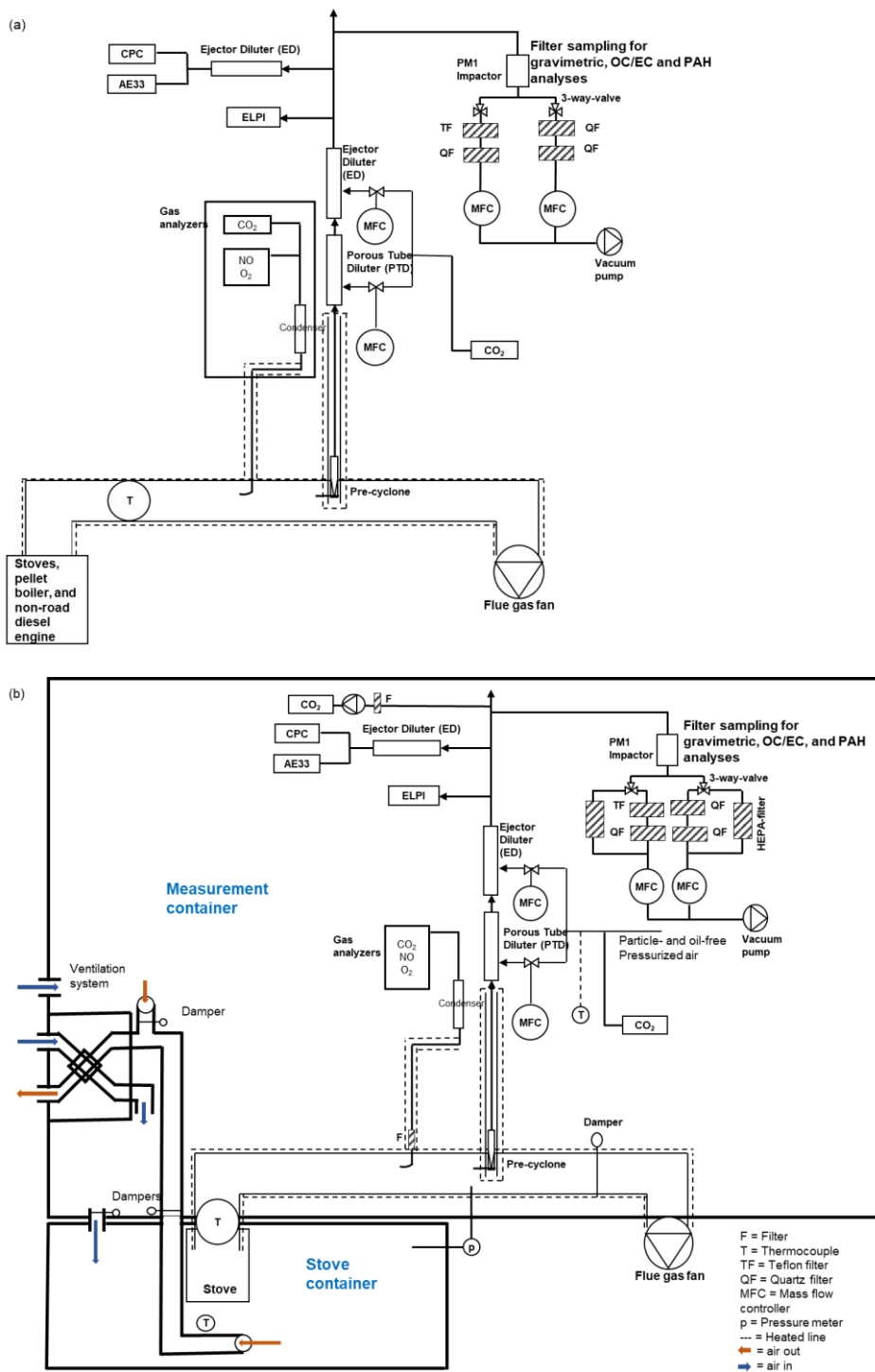
**Figure S1.** Schematics of the experimental setup at a) ILMARI and b) SIMO (modified from Tissari et al. (2019)).
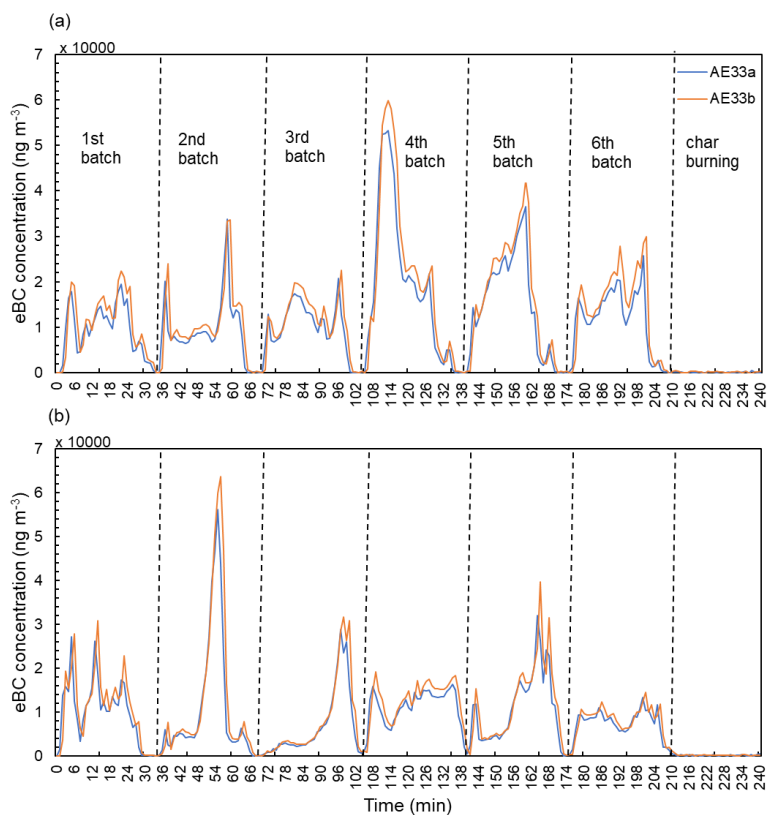
**Figure S2.** Comparison of black carbon concentration raw data between the two AE33 instruments used in this work. The concentrations are without DR correction and originate from two individual MCS experiments in ILMARI 2021 experiments.

**Table S2.** Fuel types burnt in different appliances along with the fuel moisture content, Air-to-fuel ratio, DR after the first dilution step, and modified combustion efficiency (MCE) are reported as averages (± average of standard deviations during the experiments) for all experiments.

| Appliance | Abbrv | Measurement site and date | fuel type | fuel moisture content | number of repetitions | number of batches | Air-to-fuel ratio | DR | MCE |
|---|---|---|---|---|---|---|---|---|---|
| Modern masonry heater | MMH | ILMARI 2013 | beech | 9 % | 4 | 6 | $5.21 \pm 1.47$ | $37.36 \pm 6.34$ | $0.98 \pm 0.02$ |
| | | | spruce | 7.4 % | 3 | 6 | $4.03 \pm 0.65$ | $37.28 \pm 5.95$ | $0.97 \pm 0.04$ |
| | | | birch | 7.2 % | 6 | 6 | $3.84 \pm 0.43$ | $36.23 \pm 3.37$ | $0.98 \pm 0.03$ |
| Conventional masonry heater | CMH | SIMO 2019 | birch | 11 % | 3 | 3–4 | $2.82 \pm 0.29$ | $89.81 \pm 0.20$ | $0.98 \pm 0.01$ |
| Sauna stoves (10 types) | SS-11 | SIMO 2018 | birch | 11 % | 23 | 3 | $2.55 \pm 0.41$ | $87.91 \pm 7.91$ | $0.97 \pm 0.02$ |
| | SS-18 | | birch | 18 % | 12 | 3 | $2.81 \pm 0.39$ | $72.97 \pm 17.76$ | $0.95 \pm 0.01$ |
| | SS-28 | | birch | 28 % | 3 | 3 | $2.68 \pm 0.17$ | $91.72 \pm 2.52$ | $0.94 \pm 0.002$ |

| | | | | | | | | | |
|---|---|---|---|---|---|---|---|---|---|
| Modern chimney stove | MCS | ILMARI 2016 | pine | 6.1 % | 3 | 5 | 2.79 ± 0.23 | 13.74 ± 0.49 | 0.98 ± 0.01 |
| | | | spruce | 7.4 % | 3 | 5 | 2.76 ± 0.27 | 23.37 ± 7.29 | 0.98 ± 0.01 |
| | | ILMARI 2021 | beech | 9 % | 14 | 6 | 2.37 ± 0.37 | 57.57 ± 7.78 | 0.98 ± 0.02 |
| | | | peat | 17.9 % | 3 | 8 | 3.14 ± 0.46 | 101.09 ± 0.74 | 0.99 ± 0.01 |
| Pellet boiler | PB | ILMARI 2016 | softwood pellets | 7.3 % | 3 | 4 | 2.48 ± 0.53 | 10.13 ± 0.72 | 0.998 ± 0.002 |
| Non-road diesel engine | NrDE | ILMARI 2016 | diesel | | 3 | 4 | 3.35 ± 1.16 | 9.75 ± 1.24 | 0.998 ± 0.001 |

**Section S1 Determination of the BrC fraction**

30   The contribution of brown carbon to the total aerosol absorption ($BrC_{370-950}$) was calculated based on the absorption coefficients measured by the seven-wavelength aethalometer. Using the experiment-type-wise averaged absorption coefficients, we establish parameters labelled total dimensionless integrated absorption of the total aethalometer wavelength range ($DIA_{Tot}$), BC ($DIA_{BC}$), and BrC ($DIA_{BC}$). In the following, this calculation is presented step-by-step first in general, then for a specific example case of a modern chimney stove (MCS).

35   **a) Determination of the total dimensionless integrated absorption ($DIA_{Tot}$).** A power law function is fit to the absorptions measured at the seven aethalometer wavelengths using the least squares method.

$$b_{abs,fit}(\lambda) = B_{abs,fit}(880nm) \times \left(\frac{\lambda}{880\ nm}\right)^{-AAE_{370-950}} \tag{S1}$$

Where $B_{abs,fit}(880nm)$ represents the absorption by BC at 880 nm, with the unit $m^{-1}$. $DIA_{tot}$ is then computed as the definite integral over the wavelength range of $\lambda_1 = 370$ nm to $\lambda_2 = 950$ nm.

40   $$DIA_{Tot} = \int_{\lambda_1}^{\lambda_2} B_{abs,fit}(880nm) \times \left(\frac{\lambda}{880\ nm}\right)^{-AAE_{370-950}} d\lambda = \frac{B_{abs,fit}(880nm) \times 880\ nm^{AAE_{370-950}}}{-AAE_{370-950}+1} \times (950\ \text{nm}^{-AAE_{370-950}+1} -$$
$$370\ \text{nm}^{-AAE_{370-950}+1}) \tag{S2}$$

**b) Determination of the dimensionless integrated absorption by BC ($DIA_{BC}$)** by computing the definite integral of the BC function (eq. S3) over the wavelength range of 370 nm to 950 nm. Here, an $AAE_{BC}$ of 1 was applied.

$$b_{abs}(BC,\lambda) = b_{abs}(880nm) \times \left(\frac{\lambda}{880\ nm}\right)^{-AAE_{BC}} \tag{S3}$$

45   $$DIA_{BC} = \int_{\lambda_1}^{\lambda_2} b_{abs}(880nm) \times \left(\frac{\lambda}{880\ nm}\right)^{-1} d\lambda = b_{abs}(880nm) \times 880\ nm \times \ln\left(\frac{950nm}{370nm}\right) \tag{S4}$$

**c) Determination of the dimensionless integrated absorption by BrC ($DIA_{BrC}$)** as the difference between $DIA_{tot}$ and $DIA_{BC}$.

$$DIA_{BrC} = DIA_{Tot} - DIA_{BC} \tag{S5}$$

**d) The total contribution of brown carbon to the aerosol absorption** ($BrC_{370-950}$) is then defined as the ratio of $DIA_{BrC}$ to $DIA_{Tot}$.

50 $$BrC_{370-950} = \frac{DIA_{BrC}}{DIA_{Tot}} \tag{S6}$$

**Example calculation:** The calculation of the DIAs demonstrated in Figure S3(a–c) for the case of MCS use. The total absorption is represented by the following function: $b_{abs}(\lambda) = 0.55\ m^{-1} \times \left(\frac{\lambda}{880\ nm}\right)^{-1.201}$, as illustrated in Figure S3a. Integrating this function over the wavelength range of 370 nm to 950 nm, as shown in Eq. (S2), we get the $DIA_{Tot}$ of 495.5 $\times 10^{-9}$. In Fig. S3a, $DIA_{Tot}$ is represented by the orange area.
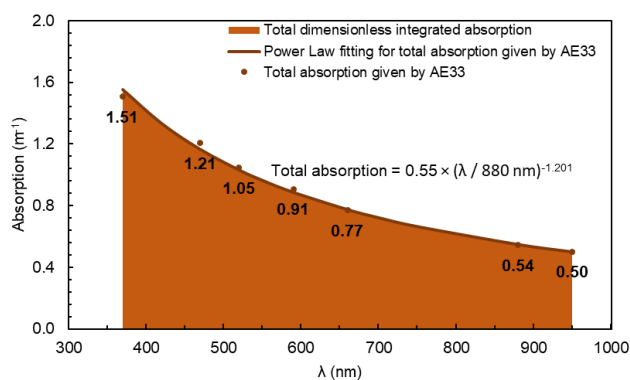
55

**Figure S3a.** Total absorptions ($m^{-1}$) given by AE33 at the seven wavelengths (brown marker), the power law fitting for the total absorption (brown line), and the $DIA_{Tot}$ (orange area). The numbers in the graph are the total absorption coefficients ($m^{-1}$) given by AE33 for the individual wavelengths (370–950 nm).

For calculation of the $DIA_{BC}$ of each experiment type, the $b_{abs}(880\ nm)$ value is determined as the average absorption 60 coefficient at 880 nm. $DIA_{BC}$ (shown as a grey area in Fig. S3b) is calculated by integrating Eq. (S4) over a wavelength range of 370 nm to 950 nm. With the average $b_{abs}(880\ nm)$ of 0.54 $m^{-1}$ for MCS, including all the different fuel types, the $DIA_{BC}$ was $452.5 \times 10^{-9}$ for MCS.
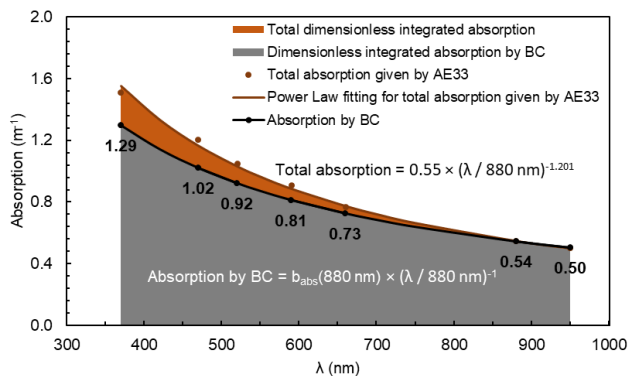
**Figure S3b.** In addition to Fig. S3a, the absorption by BC when $AAE_{BC} = 1$ is shown in a black line. The $DIA_{BC}$ is represented with a grey area. The numbers in the graph are the absorption by BC ($m^{-1}$) at individual wavelengths (370–950 nm) calculated with $AAE_{BC} = 1$.

$DIA_{BrC}$ is then calculated as the difference between $DIA_{Tot}$ and $DIA_{BC}$. In Fig. S3c, $DIA_{BrC}$ is represented as a yellowish-brown area. For MCS, the $DIA_{BrC}$ value was $43.9 \times 10^{-9}$. The total contribution of BrC to the light absorption is then calculated as the ratio of $DIA_{BrC}$ to $DIA_{Tot}$, resulting in $BrC_{370-950}$ of 8.9 % for MCS.
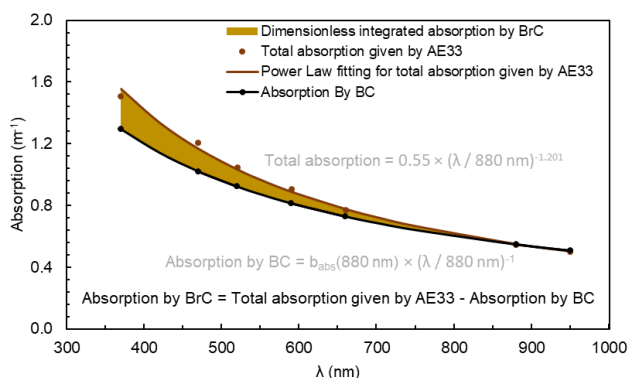
**Figure S3c.** The dimensionless integrated absorption ($DIA_{BrC}$), defined as the difference between $DIA_{Tot}$ (Fig. S3a) and $DIA_{BC}$ (Fig. S3b), is illustrated as the yellowish-brown area.

**Table S3.** The range of estimated relative uncertainty of $AAE_{470/950}$ in different combustions experiments. *Sauna stoves are presented as SSX_YY, where X represents different stoves (1-10) and YY represents the fuel moisture content (11-28 %).

| Appliance | Abbrv. | Measurement site and date | fuel type | 1 min average | Batch wise average | Whole experiment average |
|---|---|---|---|---|---|---|
| Modern masonry heater | MMH | ILMARI 2013 | beech | 0–179 | 0.1–2.1 | 0.1–0.8 |
| | | | spruce | 0–72 | 0.1–0.7 | 0.1–0.2 |
| | | | birch | 0–1206 | 0.4–6.3 | 0.3–2.1 |

| | | | | | | |
|---|---|---|---|---|---|---|
| Conventional masonry heater | CMH | SIMO 2019 | birch | 0–13352 | 0.9–10.9 | 1.8–3.9 |
| Sauna stoves* (10 types) | SS1_11 | SIMO 2018 | birch | 0–7118 | 0.4–8.9 | 1.6–3.8 |
| | SS1_18 | | birch | 0–11568 | 1.3–11.0 | 1.6–3.6 |
| | SS2_17 | | birch | 0–2925 | 1.4–8.1 | 2.0–3.8 |
| | SS3_17 | | birch | 0–8070 | 3.7–13.3 | 2.8–7.3 |
| | SS4_11 | | birch | 0–359917 | 10.4–76.0 | 12.2–34.0 |
| | SS5_11 | | birch | 0–4491 | 0.6–6.7 | 1.7–3.7 |
| | SS6_11 | | birch | 0–15870 | 3.0–7.6 | 2.9–3.8 |
| | SS7_11 | | birch | 0–11305 | 1.6–14.2 | 1.7–4.9 |
| | SS8_11 | | birch | 0–19396 | 3.6–13.8 | 2.5–8.1 |
| | SS8_18 | | birch | 0–450743 | 1.0–11.6 | 2.1–37.5 |
| | SS8_28 | | birch | 0–7520 | 0.6–11.5 | 1.9–2.4 |
| | SS9_11 | | birch | 0–34849 | 2.8–18.1 | 1.8–6.2 |
| | SS10_11 | | birch | 0–14026 | 1.2–11.9 | 0.8–7.0 |
| Modern chimney stove | MCS | ILMARI 2016 | pine | 0–228 | 0.2–1.0 | 0.1–0.7 |
| | | | spruce | 0–173 | 0.1–0.6 | 0.1–0.5 |
| | | ILMARI 2021 | beech | 0–2000 | 0.3–8.9 | 0.4–4.3 |
| | | | peat | 0–1337 | 0.2–6.3 | 0.0–0.0 |
| Pellet boiler | PB | ILMARI 2016 | softwood pellets | 0–272 | 0.0–0.3 | 0.0–0.3 |
| Non-road diesel engine | NrDE | ILMARI 2016 | diesel | 0–104 | 0.0–0.3 | 0.1–0.1 |

**Section S2 Uncertainty in the BrC fraction**

75 The uncertainty in the relative contribution of BC and BrC to the absorption at the wavelengths measured by the aethalometer was derived based on the uncertainties in the instrument parameters. The total absorption at each wavelength measured by the aethalometer is given by Eq. S7 (Drinovec et al., 2015):

$$b_{abs,tot}(\lambda) = \frac{S(\frac{\Delta ATN_{880nm}}{100})}{F(1-Z)C(1-k_\lambda \times ATN_\lambda)\Delta t} \tag{S7}$$

Where S, F, Z, and C are instrument-dependent constants for spot surface area, volumetric flow, leaking, and multiple
80 scattering corrections, respectively. The absorption by BC is calculated for each wavelength from the attenuation at 880 nm using an $AAE_{BC} = 1$ (Eq. S8).

$$b_{abs,BC}(\lambda) = \frac{S(\frac{\Delta ATN_{880nm}}{100})}{F(1-Z)C(1-k_{880nm} \times ATN_{880nm})\Delta t} \times (\frac{\lambda}{880})^{-AAE_{BC}} \tag{S8}$$

For each wavelength, the relative fraction of absorption by BC is then given by the ratio of $b_{abs}(BC, \lambda)$ to the total $b_{abs}$ (Eq. S9).

85 $$BC(\%) = \frac{b_{abs,\,BC}(\lambda)}{b_{abs,\,tot}(\lambda)} = \frac{\frac{\Delta ATN_{880nm}}{1-k_{880nm}\times ATN_{880nm}}\times\left(\frac{\lambda}{880}\right)^{-1}}{\frac{\Delta ATN_\lambda}{1-k_\lambda\times ATN_\lambda}} = \frac{\Delta ATN_{880nm}}{1-k_{880nm}\times ATN_{880nm}} \times \frac{1-k_\lambda\times ATN_\lambda}{\Delta ATN_\lambda} \times \frac{880}{\lambda} \tag{S9}$$

and BrC by Eq. S10:

$$BrC(\%) = 1 - \frac{b_{abs,\,BC}(\lambda)}{b_{abs,\,tot}(\lambda)} = 1 - \frac{\Delta ATN_{880nm}}{1-k_{880nm}\times ATN_{880nm}} \times \frac{1-k_\lambda\times ATN_\lambda}{\Delta ATN_\lambda} \times \frac{880}{\lambda} \tag{S10}$$

The uncertainty function of the fraction of BC or BrC on each wavelength (Eq. S11) finally depends on six variables: $\Delta ATN_{880nm}, k_{880nm}, ATN_{880nm}, \Delta ATN_\lambda, k_\lambda, and\ ATN_\lambda$. Note that the absolute uncertainty is the same for both BC and BrC, 

90 while the relative uncertainty increases for the smaller quantity (typically BrC).

$$\delta f = \sqrt{\begin{array}{l}\left(\frac{\partial f}{\partial \Delta ATN_{880nm}}\right)^2 (\delta\Delta ATN_{880nm})^2 + \left(\frac{\partial f}{\partial k_{880nm}}\right)^2 (\delta k_{880nm})^2 + \left(\frac{\partial f}{\partial ATN_{880nm}}\right)^2 (\delta ATN_{880nm})^2 \\ + \left(\frac{\partial f}{\partial \Delta ATN_\lambda}\right)^2 (\delta\Delta ATN_\lambda)^2 + \left(\frac{\partial f}{\partial k_\lambda}\right)^2 (\delta k_\lambda)^2 + \left(\frac{\partial f}{\partial ATN_\lambda}\right)^2 (\delta ATN_\lambda)^2\end{array}} \tag{S11}$$

For $k_\lambda$'s, arithmetic means of complete measurements were used. The uncertainty in $k_\lambda$ $(\partial k_\lambda)$ was estimated as the standard deviation during the corresponding whole experiment (typically in the order of $10^{-4} – 10^{-5}$). Similarly to Helin et al. (2021), we simplified the uncertainty equation $\delta f$ by assuming that uncertainty in the change in ATN is the same for all wavelengths and 

95 independent of time (Backman et al., 2017):

$$\delta\Delta ATN \approx \delta\Delta ATN_\lambda \approx \delta\Delta ATN_{880nm} \tag{S12}$$

and that the uncertainty in the attenuation ($\delta$ATN) is equal to $\delta\Delta$ATN/$\sqrt{2}$. This leads to simplified uncertainty function (S13, further reordered in S14):

$$\delta f = \sqrt{\begin{array}{l}\left(\frac{\partial f}{\partial \Delta ATN_{880nm}}\right)^2 (\delta\Delta ATN)^2 + \left(\frac{\partial f}{\partial k_{880nm}}\right)^2 (\delta k_{880nm})^2 + \left(\frac{\partial f}{\partial ATN_{880nm}}\right)^2 \left(\delta\Delta ATN/\sqrt{2}\right)^2 \\ + \left(\frac{\partial f}{\partial \Delta ATN_\lambda}\right)^2 (\delta\Delta ATN)^2 + \left(\frac{\partial f}{\partial k_\lambda}\right)^2 (\delta k_\lambda)^2 + \left(\frac{\partial f}{\partial ATN_\lambda}\right)^2 \left(\delta\Delta ATN/\sqrt{2}\right)^2\end{array}} \tag{S13}$$

$$\delta f = \sqrt{ \begin{aligned} &\left( \left(\frac{\partial f}{\partial \Delta ATN_{880nm}}\right)^2 + \frac{1}{2}\left(\frac{\partial f}{\partial ATN_{880nm}}\right)^2 + \left(\frac{\partial f}{\partial \Delta ATN_\lambda}\right)^2 + \frac{1}{2}\left(\frac{\partial f}{\partial ATN_\lambda}\right)^2 \right)(\delta\Delta ATN)^2 \\ &+ \left(\frac{\partial f}{\partial k_{880nm}}\right)^2 (\delta k_{880nm})^2 + \left(\frac{\partial f}{\partial k_\lambda}\right)^2 (\delta k_\lambda)^2 \end{aligned} }$$
(S14)

100

where the partial derivatives are as follows:

$$\frac{\partial f}{\partial \Delta ATN_{880nm}} = \frac{1 - k_\lambda \times ATN_\lambda}{\Delta ATN_\lambda (1 - k_{880nm} \times ATN_{880nm})} \times \frac{880}{\lambda}$$
(S15)

$$\frac{\partial f}{\partial k_{880}} = \frac{\Delta ATN_{880nm} \times ATN_{880nm}(1 - k_\lambda \times ATN_\lambda)}{\Delta ATN_\lambda (1 - k_{880nm} \times ATN_{880nm})^2} \times \frac{880}{\lambda}$$
(S16)

$$\frac{\partial f}{\partial ATN_{880nm}} = \frac{\Delta ATN_{880nm} \times k_{880}\,(1 - k_\lambda * ATN_\lambda)}{\Delta ATN_\lambda (1 - k_{880nm} \times ATN_{880nm})^2} \times \frac{880}{\lambda}$$
(S17)

105

$$\frac{\partial f}{\partial \Delta ATN_\lambda} = -\frac{1 - k_\lambda \times ATN_\lambda}{\Delta ATN_\lambda^2 (1 - k_{880nm} \times ATN_{880nm})} \times \frac{880}{\lambda}$$
(S18)

$$\frac{\partial f}{\partial k_\lambda} = -\frac{\Delta ATN_{880nm} \times ATN_\lambda}{\Delta ATN_\lambda (1 - k_{880nm} \times ATN_{880nm})} \times \frac{880}{\lambda}$$
(S19)

$$\frac{\partial f}{\partial ATN_\lambda} = -\frac{\Delta ATN_{880nm} \times k_\lambda}{\Delta ATN_\lambda (1 - k_{880nm} \times ATN_{880nm})} \times \frac{880}{\lambda}$$
(S20)

e resulting absolute uncertainties for the contribution of BrC and BC to the absorption at the seven aethalometer wavelengths are presented in Figure S4 for the different fuel-appliance pairs.
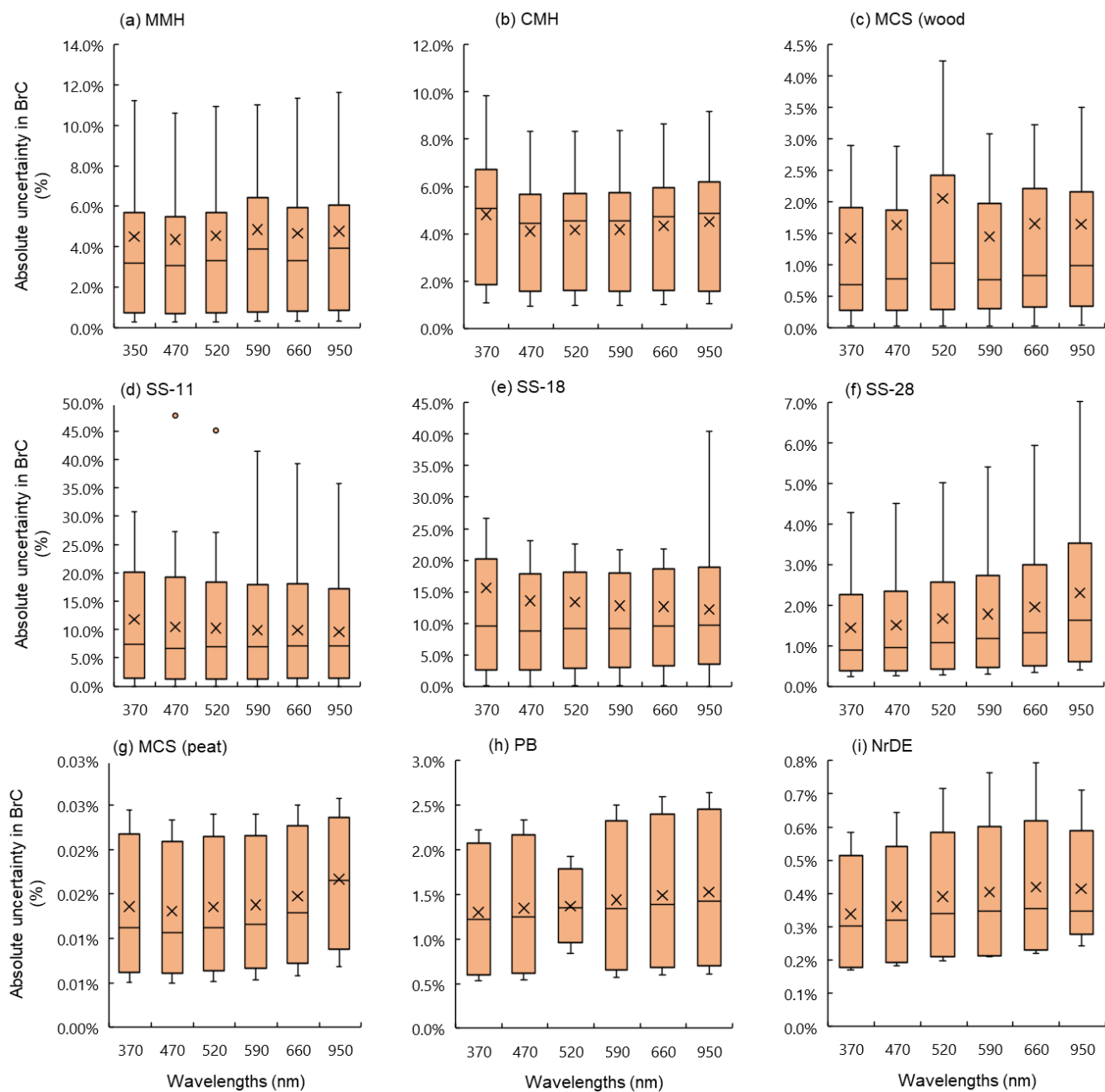
**Figure S4.** Absolute uncertainty in absorption by BrC (%) and BC based on two-wavelength measurements with $AAE_{BC} = 1$. The box edges show the 25th to 75th percentile range of experiment-wise averaged uncertainties, the vertical line shows the 50th percentile whereas the whiskers indicate the 5th to 95th percentile range. '×' indicates the arithmetic mean of the uncertainties. The absolute uncertainties are calculated from the individual experimental days except for combustion peat in MCS, which is calculated from individual batch experiments.

110
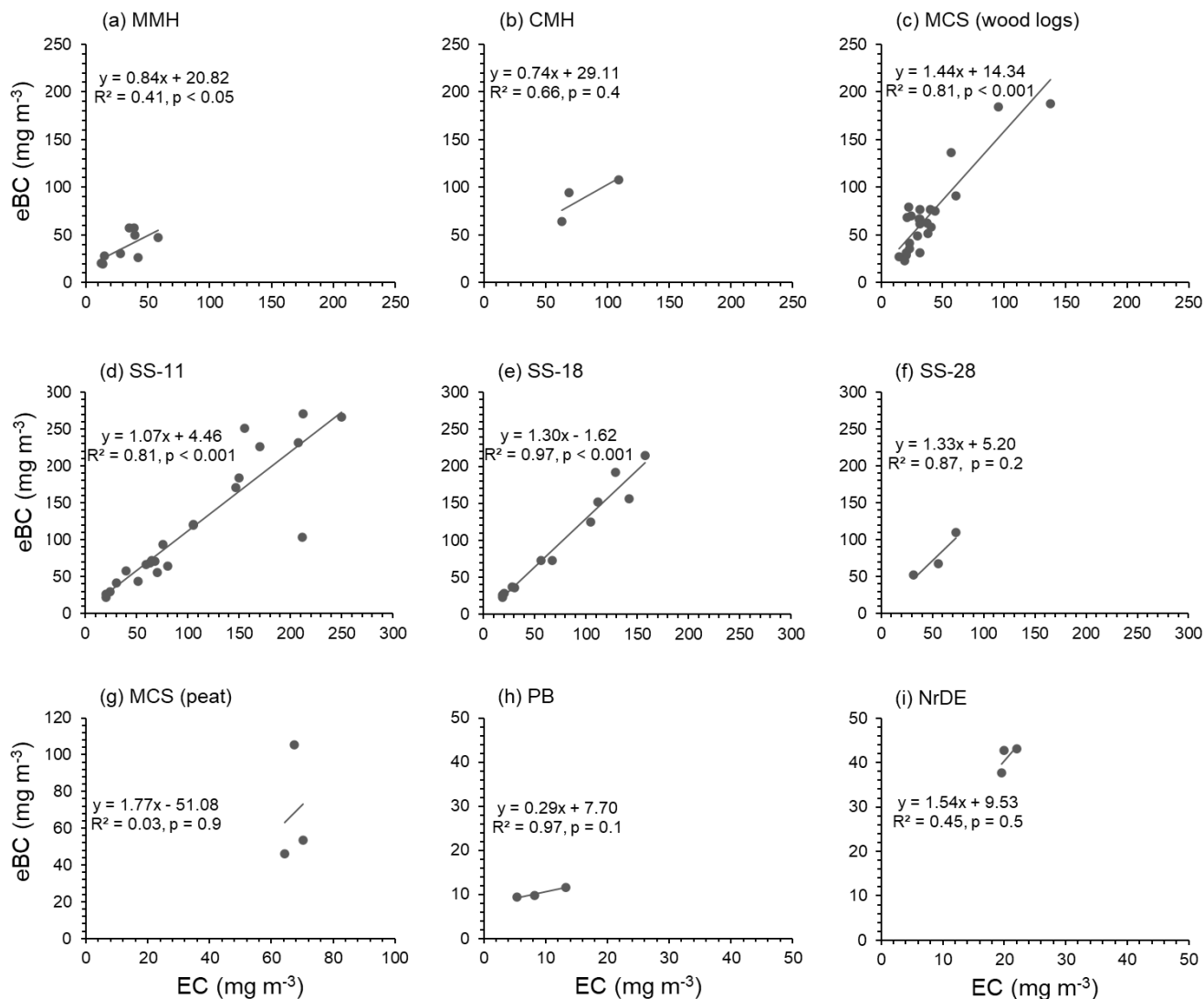
115

**Figure S5.** Comparison of the EC concentration (mg m$^{-3}$) (offline filter analysis) to the average eBC concentration (mg m$^{-3}$) (online optical measurements, AE33) in the raw gas conditions for a) MMH, b) CMH, c) MCS with wood logs, d) SS1 with birch logs with 11% moisture content, e) SS2 with birch logs with 18% moisture content, f) SS3 with birch logs with 28% moisture content, g) MCS with peat, h) PB, and i) non-road diesel engine. The solid line represents the linear regression with Pearson correlation coefficient of R) and significance of p

120 (based on the F-value of the regression). EC measurement analysis for MMH, CMH, SS, PB, and the non-road diesel engine was performed using NIOSH5040 thermal protocol while MCS was analyzed using IMPROVE-A protocol.
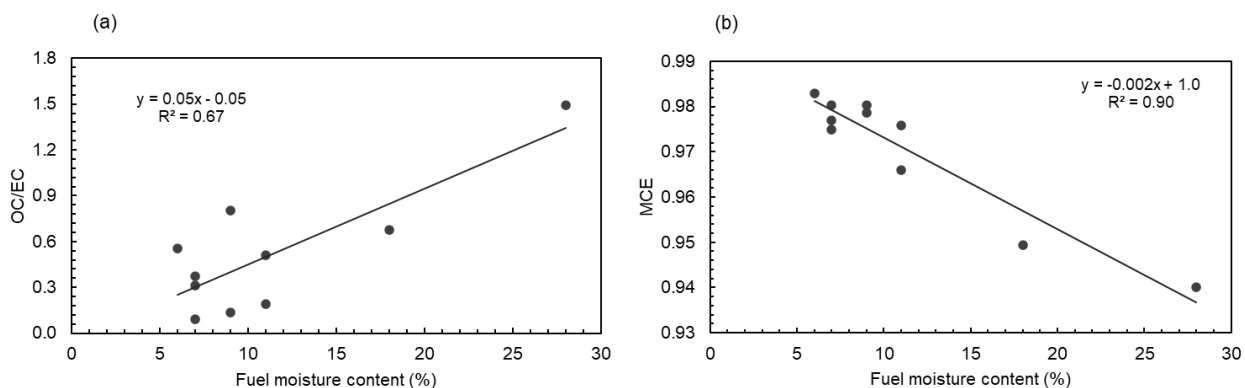
**Figure S6.** Relation between a) OC/EC and b) MCE with fuel moisture content for the averaged wood log fuel/appliance combinations.

**Table S4.** The particle size, $AAE_{470/950}$ (± STD of individual values), OC/EC ratio, and $MAC_{880nm}$ (± STD of means) for different fuel-appliance combinations.

| Appliances | Fuel types | Fuel moisture content | GMD (nm) | GSD | $AAE_{470/950}$ | OC/EC | $MAC_{880nm}$ $(m^2\ g^{-1})$ |
|---|---|---|---|---|---|---|---|
| MMH | Beech | 9% | 58.36 | 1.90 | 1.19 ± 0.40 | 0.14 ± 0.07 | 9.98 ± 4.13 |
| | Spruce | 7% | 59.73 | 1.90 | 1.22 ± 0.19 | 0.31 ± 0.24 | 12.86 ± 1.25 |
| | Birch | 7% | 66.95 | 1.95 | 1.0 ± 0.31 | 0.09 ± 0.04 | 9.00 ± 2.75 |
| CMH | Birch | 11% | 97.40 | 1.92 | 1.19 ± 0.63 | 0.19 ± 0.05 | 8.41 ± 1.34 |
| SS-11 | Birch | 11% | 115.49 | 1.98 | 1.26 ± 0.18 | 0.51 ± 0.42 | 8.56 ± 1.80 |
| SS-18 | Birch | 18% | 128.32 | 2.01 | 1.34 ± 0.36 | 0.68 ± 0.31 | 10.02 ± 0.91 |
| SS-28 | Birch | 28% | 105.74 | 2.01 | 1.61 ± 0.47 | 1.49 ± 0.16 | 11.03 ± 1.45 |
| MCS | Pine | 6% | 122.76 | 2.11 | 1.13 ± 0.20 | 0.55 ± 0.52 | 12.20 ± 2.05 |
| | Spruce | 7% | 87.16 | 2.11 | 1.24 ± 0.21 | 0.37 ± 0.15 | 13.74 ± 2.86 |
| | Beech | 9% | 81.64 | 2.00 | 1.29 ± 0.49 | 0.80 ± 0.62 | 14.01 ± 7.78 |
| | Peat | 18% | 64.36 | 1.86 | 1.18 ± 0.83 | 0.17 ± 0.05 | 7.88 ± 3.01 |
| PB | Softwood Pellet | 7% | 57.52 | 2.03 | 1.24 ± 0.12 | 0.19 ± 0.09 | 8.16 ± 2.84 |
| NrDE | Diesel | | 44.30 | 1.84 | 1.02 ± 0.05 | 0.10 ± 0.01 | 15.60 ± 0.75 |
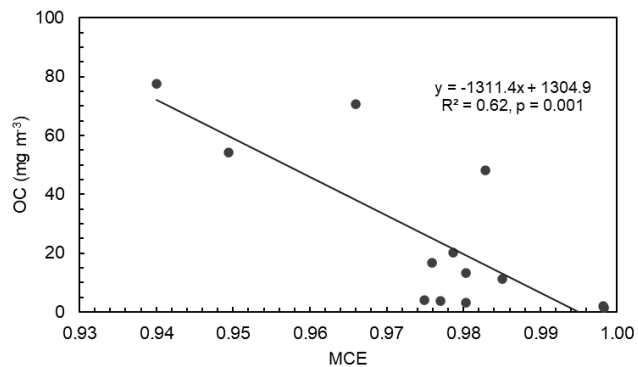
**Figure S7.** Relation between OC (mg m$^{-3}$, in raw gas conditions) and MCE for the wood log combustion appliances (average of fuel/appliance types).
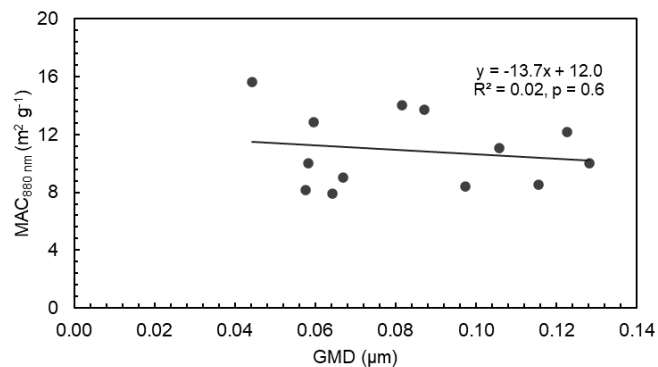
130 **Figure S8.** Relation between MAC$_{880 \, nm}$ (m$^2$ g$^{-1}$) and GMD (nm) for the wood combustion appliances (average of fuel/appliance types).
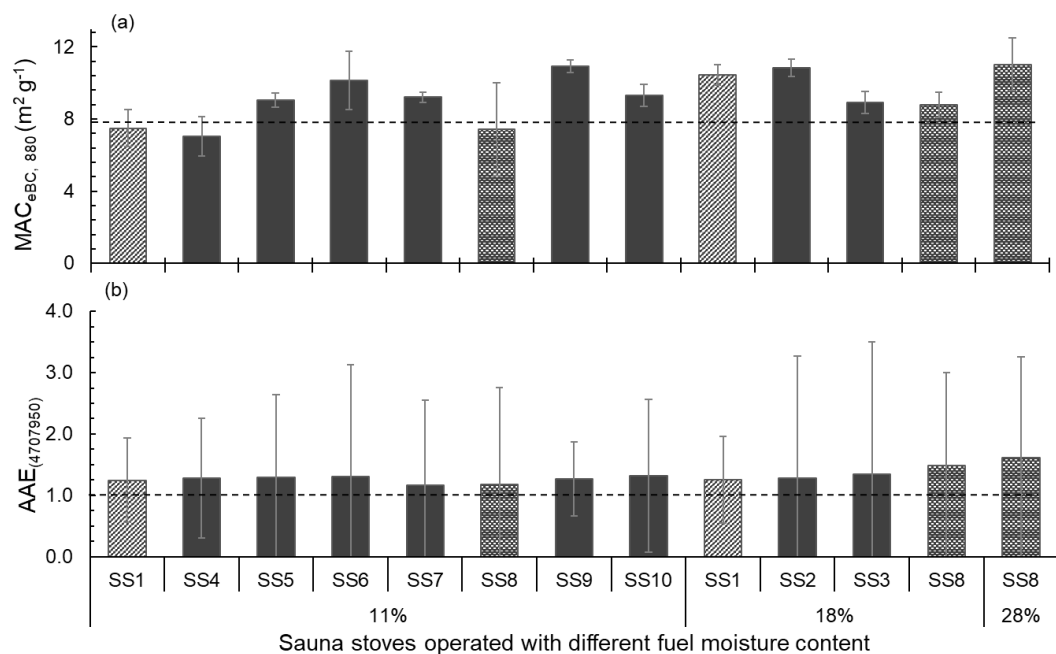
**Figure S9.** Optical properties of emissions from sauna stoves 1-10 given as SS1 to S10 operated with wood logs with different fuel moisture content (11%, 18%, and 28 %). a) MAC$_{eBC,880nm}$ (m$^2$ g$^{-1}$) (± STD) and b)AAE$_{470/950}$ (± STD) for stoves 1-10. The bars with patterns indicate the same stoves (SS1 and SS8) with fuels having different moisture content. The data are partially published in Tissari et al., (2019).

135    **Table S5.** Optical properties of the emissions from sauna stoves 1-10 given as SS1 to S10 operated with birch logs with different fuel moisture contents.

| Appliances | Fuel moisture content (%) | AAE$_{470/950}$ | MAC$_{880nm}$ | Total abs by BC (%) (AAE$_{BC}$ = 1) | Total abs by BrC (%) (AAE$_{BC}$ = 1) |
|---|---|---|---|---|---|
| SS1 | 11 | 1.2 ± 0.7 | 7.5 ± 1.0 | 94.8 | 5.2 |
| SS4 | 11 | 1.3 ± 1.0 | 7.0 ± 1.1 | 91.4 | 8.6 |
| SS5 | 11 | 1.3 ± 1.3 | 9.1 ± 0.4 | 91.7 | 8.3 |
| SS6 | 11 | 1.3 ± 1.8 | 10.1 ± 1.6 | 91.6 | 8.4 |
| SS7 | 11 | 1.2 ± 1.4 | 9.2 ± 0.3 | 98.0 | 2.0 |
| SS8 | 11 | 1.2 ± 1.6 | 7.4 ± 2.6 | 96.9 | 3.1 |
| SS9 | 11 | 1.3 ± 0.6 | 10.9 ± 0.4 | 94.2 | 5.8 |
| SS10 | 11 | 1.3 ± 1.2 | 9.3 ± 0.6 | 88.8 | 11.2 |
| SS1 | 18 | 1.3 ± 0.7 | 10.4 ± 0.6 | 90.2 | 9.8 |
| SS2 | 17 | 1.3 ± 2.0 | 10.9 ± 0.5 | 90.8 | 9.2 |
| SS3 | 17 | 1.3 ± 2.2 | 8.9 ± 0.6 | 89.8 | 10.2 |
| SS8 | 18 | 1.5 ± 1.5 | 8.8 ± 0.7 | 82.5 | 17.5 |

| | | | | |
|---|---|---|---|---|
| SS8 | 28 | 1.6 ± 1.6 | 11.0 ± 1.5 | 77.3 | 22.7 |
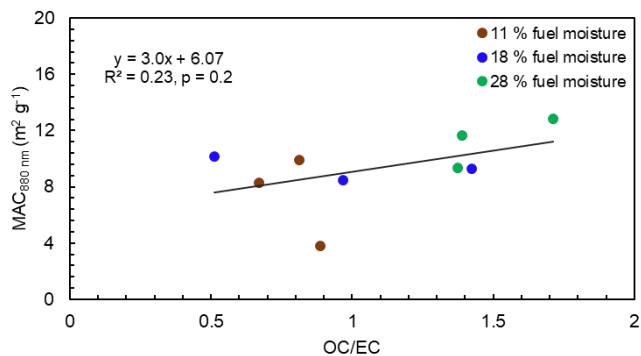
**Figure S10.** Relation between MAC$_{880\ nm}$ (m$^2$ g$^{-1}$) and OC/EC for SS8, utilizing fuel with three different moisture content.

**Table S6.** The contribution of BC (BC$_{370-950}$) and BrC (BrC$_{370-950}$) to the total absorption with AAE$_{BC}$ =1 for different fuel-appliance combinations, along with the contribution of BrC to the absorption at different wavelengths measured by the AE33.

| Appliance | Fuel type | Fuel Moisture content | BC$_{370-950}$ (%) | BrC$_{370-950}$ (%) | Contribution of BrC to the absorption at individual wavelengths (%) | | | | |
|---|---|---|---|---|---|---|---|---|---|
| | | | | | 370 nm | 470 nm | 520 nm | 590 nm | 660 nm |
| MMH | Beech | 9% | 93.22 | 6.78 | 7.73 | 12.70 | 9.33 | 7.84 | 7.93 |
| | Spruce | 7% | 91.10 | 8.90 | 14.08 | 15.16 | 10.78 | 9.14 | 8.97 |
| | Birch | 7% | 98.72 | 1.28 | -3.28 | 3.59 | 1.31 | 1.84 | 3.82 |
| CMH | Birch | 11% | 98.50 | 1.50 | -7.44 | 8.00 | 6.03 | 5.21 | 1.10 |
| SS-11 | Birch | 11% | 94.66 | 5.34 | 5.05 | 12.92 | 9.48 | 7.48 | 3.08 |
| SS-18 | Birch | 18% | 90.32 | 9.68 | 17.39 | 17.42 | 13.95 | 11.06 | 4.91 |
| SS-28 | Birch | 28% | 79.23 | 20.77 | 36.24 | 33.39 | 25.81 | 20.64 | 12.25 |
| MCS | Pine | 6% | 95.63 | 4.37 | 5.30 | 8.63 | 6.73 | 6.32 | 3.36 |
| | Spruce | 7% | 90.08 | 9.92 | 17.68 | 17.10 | 12.98 | 11.03 | 6.65 |
| | Beech | 9% | 89.96 | 10.04 | 16.55 | 18.07 | 14.22 | 12.35 | 6.53 |
| | Peat | 18% | 94.02 | 5.98 | 4.78 | 11.42 | 9.52 | 9.03 | 4.52 |
| PB | Softwood Pellet | 7% | 90.33 | 9.67 | 19.38 | 15.97 | 10.83 | 8.61 | 4.45 |
| NrDE | Diesel | | 99.34 | 0.66 | 5.04 | 3.14 | -0.82 | -1.32 | -2.66 |
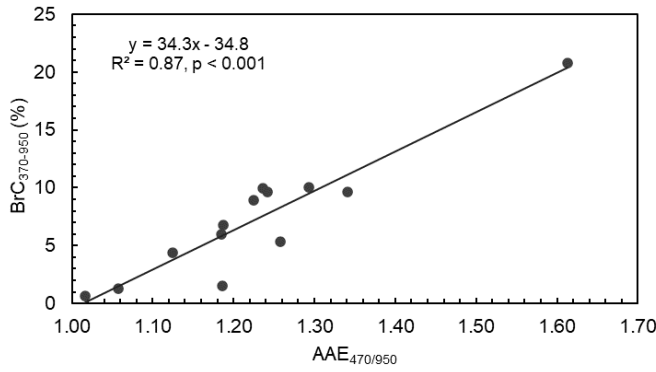
**Figure S11.** Relation between absorption by BrC$_{370-950}$ (%) and AAE$_{470/950}$.

**Section S3 Impact of the choice of AAE$_{BC}$ on the contribution of BrC to the total absorption**

The contribution of BrC to the total absorption (BrC$_{370-950}$) depends on the choice of AAE$_{BC}$. Typically, AAE$_{BC}$ =1 is used; if the actual AAE$_{BC}$ differs from this, the change in the determined BrC$_{370-950}$ is described as:

$$change\ in\ the\ BrC_{370-950nm} = \frac{1-R\times BC_{1,}-BrC_{1,\%}}{BrC_{1,\%}} \tag{S21}$$

where, BC$_1$ and BrC$_1$ are the fractional contributions of BC and BrC to the total absorption, respectively, with AAE$_{BC}$ =1, so that BC$_1$ + BrC$_1$ = 1. R is the ratio of the BC absorption with the alternative AAE (AAE$_2$) to that with AAE$_{BC}$ =1. In the range of 370 – 950 nm, the ratio R can be derived from the definition of BC as:

$$R = \frac{\int_{370\ nm}^{950\ nm} b_{abs,880nm}\times\left(\frac{\lambda}{880}\right)^{-AAE_2} d\lambda}{\int_{370\ nm}^{950\ nm} b_{abs,880nm}\times\left(\frac{\lambda}{880}\right)^{-1} d\lambda} = \frac{880^{AAE_2-1}\times\left(950^{-AAE_2+1}-370^{-AAE_2+1}\right)}{(-AAE_2+1)\times\ln\left(\frac{950}{370}\right)} \tag{S22}$$

The sensitivity of BrC$_{370-950}$ on the AAE depends on the amount of BrC in the exhaust, as illustrated in Fig S11 for AAE$_{BCS}$ 0.9 and 1.1.
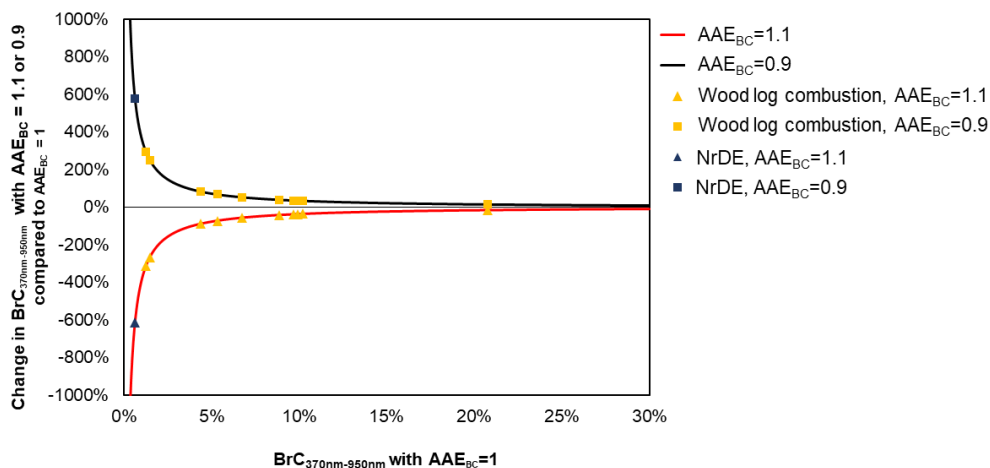
155

**Figure S12.** Change in the contribution of BrC to the total absorption in the wavelength range 370 nm - 950 nm (BrC$_{370\text{-}950}$) when AAE$_{BC}$ is changed from 1.0 to 0.9 or 1.1.
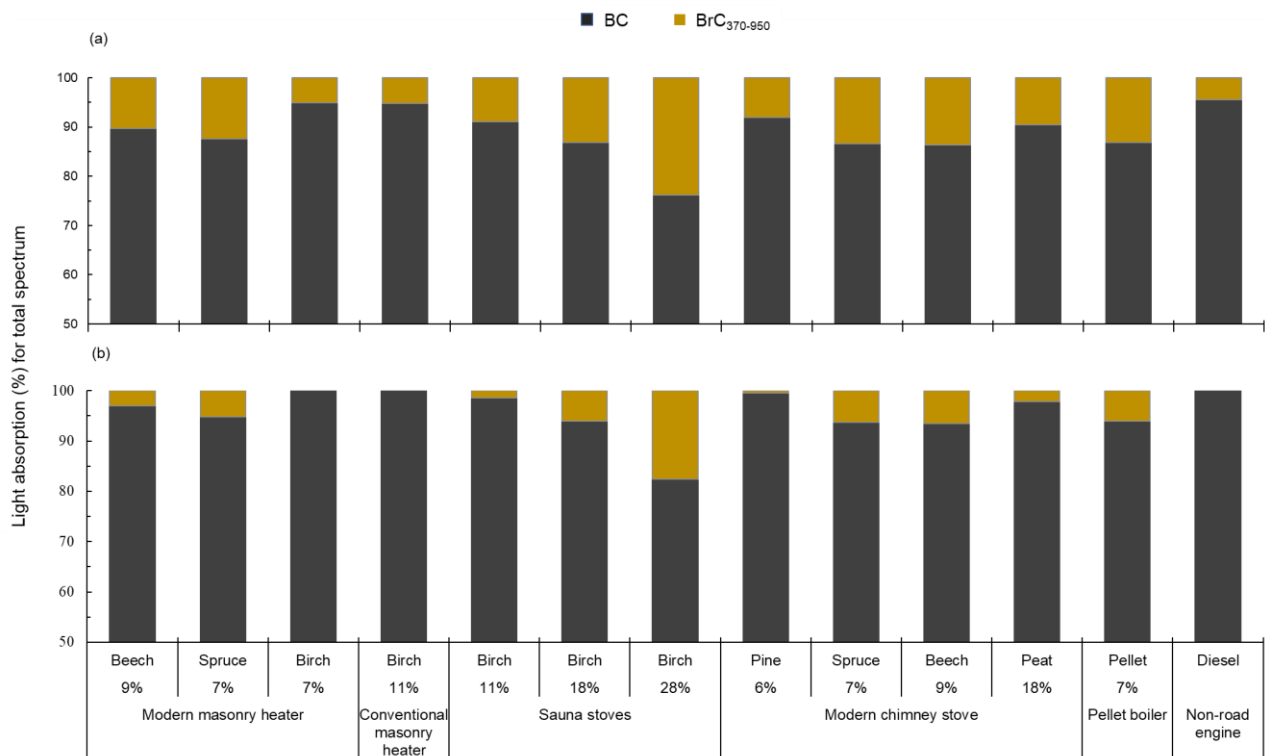
**Figure S13.** Change in BrC$_{370\text{-}950}$ contribution for different fuel types and combustion appliances when a) AAE = 0.9 and b) AAE = 1.1. The
160   percentages shown indicate the fuel moisture content.
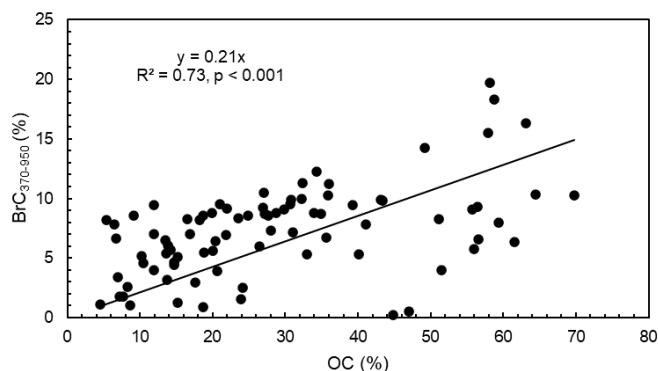
**Figure S14.** Relation between OC (%) and total $BrC_{370-950}$ (%) for individual experiments.

### References

Backman, J., Schmeisser, L., Virkkula, A., Ogren, J. A., Asmi, E., Starkweather, S., Sharma, S., Eleftheriadis, K., Uttal, T.,
165 Jefferson, A., Bergin, M., Makshtas, A., Tunved, P., and Fiebig, M.: On Aethalometer measurement uncertainties and an instrument correction factor for the Arctic, Atmos. Meas. Tech., 10, 5039–5062, 10.5194/AMT-10-5039-2017, 2017.

Drinovec, L., Močnik, G., Zotter, P., Prévôt, A. S. H., Ruckstuhl, C., Coz, E., Rupakheti, M., Sciare, J., Müller, T., Wiedensohler, A., and Hansen, A. D. A.: The "dual-spot" Aethalometer: An improved measurement of aerosol black carbon with real-time loading compensation, Atmos. Meas. Tech., 8, 1965–1979, 10.5194/amt-8-1965-2015, 2015.

170 Helin, A., Virkkula, A., Backman, J., Pirjola, L., Sippula, O., Aakko-Saksa, P., Väätäinen, S., Mylläri, F., Järvinen, A., Bloss, M., Aurela, M., Jakobi, G., Karjalainen, P., Zimmermann, R., Jokiniemi, J., Saarikoski, S., Tissari, J., Rönkkö, T., Niemi, J. V., and Timonen, H.: Variation of Absorption Ångström Exponent in Aerosols From Different Emission Sources, J. Geophys. Res. Atmos., 126, e2020JD034094, 10.1029/2020JD034094, 2021.

Tissari, J., Väätäinen, S., Leskinen, J., Savolahti, M., Lamberg, H., Kortelainen, M., Karvosenoja, N., and Sippula, O.: Fine
175 particle emissions from sauna stoves: Effects of combustion appliance and fuel, and implications for the Finnish emission inventory, Atmosphere (Basel)., 10, 775, 10.3390/ATMOS10120775, 2019.